MTLA 28 (2023) 101759

Contents lists available at ScienceDirect

Materialia

journal homepage: www.elsevier.com/locate/mtla

Full Length Article

Magnetic circular dichroism of Co nanoparticles localized in matrices of various types

Yulia Samoshkina [a,*], Irina Edelman [a], Hsiung Chou [b,c], Dmitry Petrov [a], Sergey Zharkov [a,d], Dmitry Neznakhin [e], Elena Stepanova [e], Andrey Stepanov [f]

[a] Kirensky Institute of Physics, Federal Research Center KSC SB RAS, Krasnoyarsk, Russia
[b] Department of Physics, National Sun Yat-sen University, 80424 Kaohsiung, Taiwan
[c] Department of Applied Physics, National University of Kaohsiung, 81148 Kaohsiung, Taiwan
[d] Siberian Federal University, Krasnoyarsk, Russia
[e] Institute of Natural Sciences and Mathematics, Ural Federal University, Yekaterinburg, Russia
[f] Zavoisky Physical-Technical Institute, FRC Kazan Scientific Center RAS, Kazan, Russia

ARTICLE INFO

Keywords:
Co nanoparticles
SiO_2 matrix
ZnO matrix
Magneto-optics
Absorption

ABSTRACT

Magnetic and magneto-optical properties of cobalt nanoparticles (Co-NPs) dispersed in a transparent dielectric SiO_2 and semiconductor ZnO matrices have been investigated. Field and temperature dependences of the samples magnetization showed the typical behavior of an ensemble of superparamagnetic particles with a blocking temperature near and below room temperature. The spectroscopy of magnetic circular dichroism (MCD) in the visible and near-infrared light ranges has revealed a significant difference between the behavior of the Co-NPs and a solid Co film. It has been found that the MCD spectrum shape for the Co-NPs does not depend on the matrix type. The room temperature magneto-optical activity of the Co-NPs in the different matrices has been estimated as an indicator for practical applications.

1. Introduction

The study of ensembles of transition metal nanoparticles in dielectric or semiconductor matrices is a promising task for the development of high-speed optical and magnetic recording devices [1–3]. Therefore, the magneto-optical (MO) properties of such materials are of particular interest in this direction, despite the fact that little attention has been paid to them so far. It is known that the physical properties of magnetic nanoparticles differ from both bulk and thin-film structures. The size effect can sometimes lead to unexpected results. The structural, magnetic and electron transport properties of cobalt nanoparticles (Co-NPs) have been widely studied [1,4-7]. The materials under study have exhibited promising physical properties for a wide range of applications. The MO effects such as Kerr and Faraday rotation for the Co-NPs in different dielectric matrices have been investigated previously [8–10]. A significant difference was found in the spectral dependencies of these effects compared to a solid Co film and is associated with the behavior of conduction electrons inside the particles. Besides, it was revealed that the MO spectra depend on the size and concentration of the Co-NPs. Thus, MO properties can be controlled by changing these parameters.

The present work is devoted to the study of the Co-NPs using magnetic circular dichroism (MCD) spectroscopy in the visible and near-infrared light ranges. MCD is the MO effect that observed in transmitted light and is characterizes the medium absorption [11]. This effect is more informative than the effects Kerr and Faraday, since it directly reflects the behavior of the off-diagonal component of the permittivity tensor. Besides, the MCD linearly depends on the sample magnetization and eliminates the contribution of a non-magnetic component (substrate/matrix). Two types of matrix were considered as a medium for the nanoparticles, namely dielectric (SiO_2) and semiconductor (ZnO). This choice is justified by the fact that systems of Co–ZnO and Co-NPs in SiO_2 have been extensively studied for the past two decades [4-7,12-15].

High-hydrogenated Co-doped ZnO films have been investigated previously [16]. The study showed that due to the chemical reaction of H_2 with ZnO, metallic cobalt is formed in the samples as a secondary phase. Based on the above, the high-hydrogenated Co-doped ZnO films were selected as one of the main research samples. A comparative analysis of the MCD data for the selected samples led to weighty conclusions.

* Corresponding author.
E-mail address: uliag@iph.krasn.ru (Y. Samoshkina).

https://doi.org/10.1016/j.mtla.2023.101759
Received 21 November 2022; Accepted 27 March 2023
Available online 28 March 2023
2589-1529/© 2023 Acta Materialia Inc. Published by Elsevier B.V. All rights reserved.

2. Materials and methods

Co-NPs in an amorphous SiO_2 matrix were synthesized by Co^+ ions implantation with energy of 40 keV. The current density in the ion beam was 1 μA/cm^2. The ion dose was $Q*10^{17}$ ions/cm^2, where $Q = 0.5$, 1 and 1.25. Implantation was carried out at room temperature in a vacuum with a residual pressure of 10^{-5} Torr on an ion beam accelerator ILU-3 [17]. The Co-NPs in SiO_2 (CSO) with $Q = 0.5$, 1 and 1.25 will be further designated as CSO1-CSO3, respectively.

The Co-doped ZnO (CZO) films were grown on glass substrate by the radio frequency (RF) magnetron sputtering system [16]. The films deposition was carried out at a total pressure of 30 mTorr and a forward RF power of 80 W in the atmosphere of Ar + 20% H_2 and Ar + 30% H_2 mixed gas. The substrate temperature was 450 °C. Deposition time was 20 min. The crystal structure and chemical composition of the films have been studied in detail [16]. The element-selective XANES spectroscopy at the Co K-edge (Fig. 1) revealed the presence of metallic cobalt in the samples [16]. In combination with data of X-ray fluorescent analysis (XRFA), the relative content of metallic cobalt in the films was calculated (Table 1). It should be noted that the X-ray diffraction patterns for the obtained films exhibited diffraction peaks corresponding only to the ZnO lattice and did not show the presence of a secondary phase.

Morphology of the CSO samples was studied using a high resolution transmission electron microscope (HRTEM) JEOL JEM-2100 (thermionic LaB_6 cathode) with an accelerating voltage of 200 kV. Selected-area electron diffraction (SAED) was used to determine the crystal structure of the samples. Magnetic measurements were performed using a Quantum Design MPMS-XL7 EC SQUID magnetometer in the temperature range 5–320 K and magnetic field (H) up to 12 kOe applied parallel to the film plane. The total optical density (D) spectra of the samples were measured at room temperature with the SHIMADZU-3600 instrument. The MCD spectra were measured in the normal geometry: the magnetic vector and the light beam were directed normal to the sample plane. The modulation of the polarization state of the light wave from the right-hand (D+) to the left-hand (D-) circular polarization relatively to the magnetic field direction was used. The MCD signal (ΔD) was measured as the difference between the optical densities of the right and left polarized waves in the transmitted light. The spectral range was 1.1–4.5 eV. Magnetic field reached 12 kOe. The measurement accuracy was about 10^{-4}, and the spectral resolution was 20–50 cm^{-1} depending on the wavelength.

Table 1
The films thickness and Zn/Co ratio according to XRFA. These data are consistent with the results of other research methods [16]. The specified content of metallic cobalt in the films was calculated using a combination of XRFA and XANES data.

Sample	Gas mixture	Film thickness, nm	Zn/Co	Co/(Co+Zn),% (Δ = ± 0.05)	Metallic Co (x),%
CZO1	Ar + 20% H_2	71.7	4.3	18.9	7.6 ± 0.9
CZO2	Ar + 30% H_2	53.5	3.6	21.7	13±1.1

3. Results and discussion

An example of the cross-section TEM image for the CSO2 samples is shown in Fig. 2 left. The isolated Co-NPs having a predominantly spherical shape with a diameter of 5–10 nm are observed well in the thin near-surface layer. The total film thickness was 55 nm while the cobalt nanoparticles were concentrated in the central region of the about 30 nm. The particles density in the implanted layer increases with an increase in the implantation dose. The set of the diffraction reflections observed at the selected area electron diffraction pattern (SAED) (Fig. 2 right) corresponds to the Co hexagonal close-packed (hcp) crystal structure (space group: $P6_3/mmc$; lattice constants: $a = 2.507$ Å, $c = 4.0686$ Å, PDF 4+ card #04-001-3273). The hcp phase for Co-NPs in SiO_2 was characteristic for the as-implanted samples with energy of 35 keV [18]. Analysis of the HRTEM images obtained from the CSO samples (see Fig. 2 left) shows that some of Co-NPs have a less dense core. This structure type is due to the Kirkendall effect. A similar morphology was observed on the Ni-NPs synthesized in SiO_2 matrix by implantation of Ni^+ ions [19].

According to the data on the particle size distribution (Fig. 3 for example), the average size of Co-NPs, ⟨D⟩, in the CSO1-CSO3 samples is 4.4, 6.8, and 8.5 nm, respectively. The HRTEM data concerning the shape and sizes of the particles is consistent with that of other authors [4,6]. For comparison, we also shown the size distribution of Co-NPs in SiO_2 synthesized by a similar technique at the current densities $j = 8$ μA/cm^2 and studied earlier [9]. The data presented in Fig. 3 for the samples synthesized at current densities $j = 1$ μA/cm^2 and $j = 8$ μA/cm^2 with the same ion dose indicate that the current decrease causes an increase in ⟨D⟩ and broadening of the distribution curve.

A less unambiguous situation occurs in the case of the CZO samples. A typical example of a cross-section HRTEM image of the CZO2 sample is

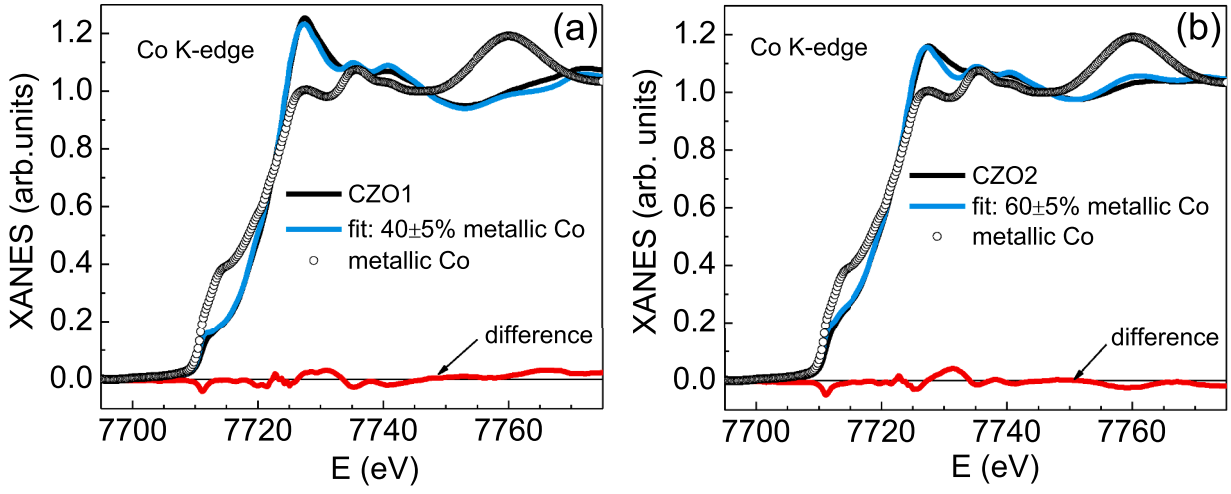

Fig. 1. Experimental Co K-edge XANES spectra for the Co-doped ZnO films at $H_2 = 20\%$ (a) and $H_2 = 30\%$ (b) together with the XANES transform data fitted to the partial content of metallic Co in the samples. The reference XANES spectrum of metallic Co is also shown for comparison.

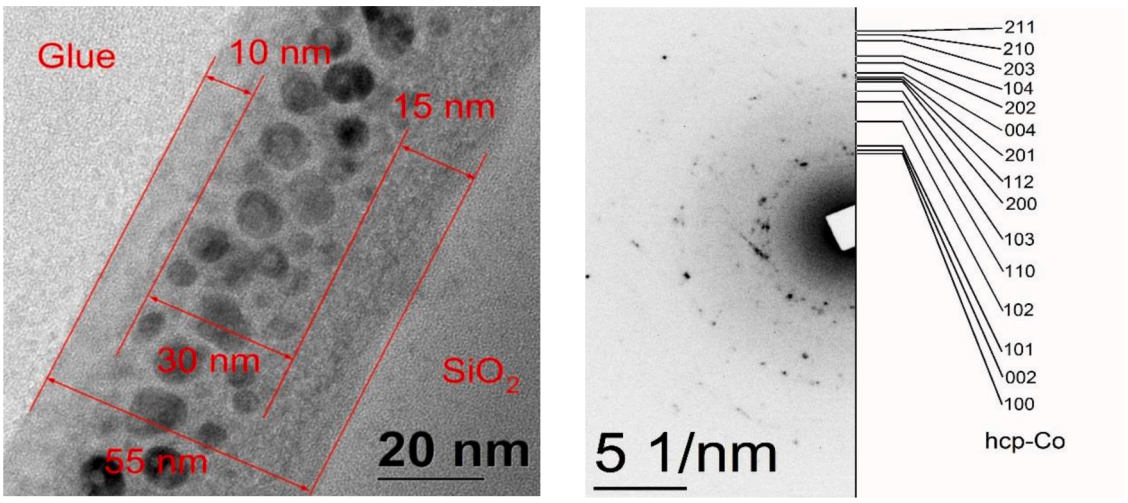

Fig. 2. Cross-section bright-field HRTEM image (left) and SAED pattern (right) for the Co-NPs in SiO_2 at the ion implantation dose of 1×10^{17} ions/cm^2.

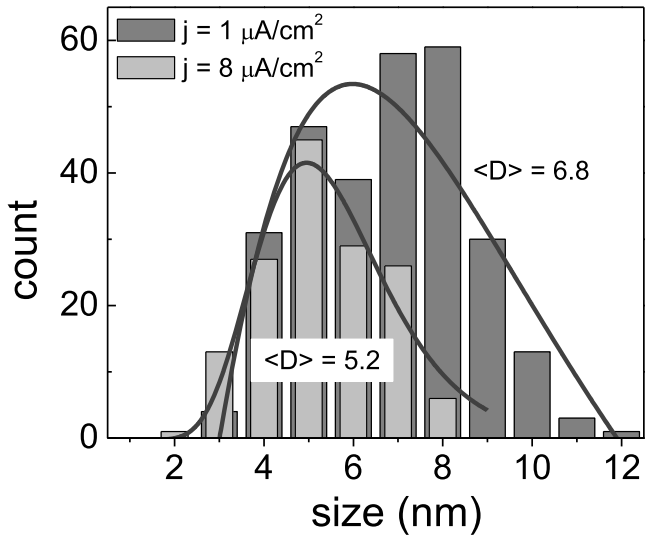

Fig. 3. The histograms of nanoparticles size distribution in the systems of Co-NPs in SiO_2 synthesized at different current density in the ion beam with an ion dose of 1×10^{17} ions/cm^2. Histograms adjusted by log-normal curves.

shown in Fig. 4 left. Analysis of the SAED pattern (Fig. 4 right) revealed the presence of the predominantly polycrystalline ZnO phase (space group: $P6_3mc$; lattice constants: $a = 3.25$ Å, $c = 5.207$ Å, PDF 4+ card #04-003-2106). Low intensity reflections corresponding to hcp-Co are also present in the SAED pattern. However, analysis of the HRTEM images (Fig. 4 on the left) do not allow identification of individual Co-NPs. The main problem is that the Co nanoparticles are located in the ZnO matrix having the polycrystalline nature. Analysis of the HRTEM data using the fast Fourier transform (FFT) also did not provide reliable information about the Co-NPs in ZnO.

Temperature dependences of the magnetization for the studied samples were measured in two cooling modes (ZFC - zero field cooled and FC - field cooled) and are shown in Fig. 5. The ZFC curves for the CSO and CZO samples are typical of an ensemble of superparamagnetic nanoparticles with a blocking temperature (T_b) that varies from sample to sample in wide range. The average particle size in the presented matrixes was estimated by the Bean-Livingston formula $T_b = K_{eff}(4\pi r^3/3)/25k_B$ [20], where K_{eff} is the energy of the effective magneto-crystalline anisotropy, k_B is Boltzmann's constant, and r is the NPs radius. According to the SAED data, Co-NPs in SiO_2 samples have hcp crystal structure. Thus, the anisotropy constant of the hcp-Co equal to 4.3×10^5 J/m^3 [21] was chosen for the estimation. The $\langle D \rangle$ value in the CSO1-CSO3 samples is ~ 5 nm ($T_b = 81$ K), 7.6 nm ($T_b = 281$ K), and 7.7 nm ($T_b = 300$ K), respectively. These values agree well with the electron microscopy data. The average size of the Co-NPs for the CZO1

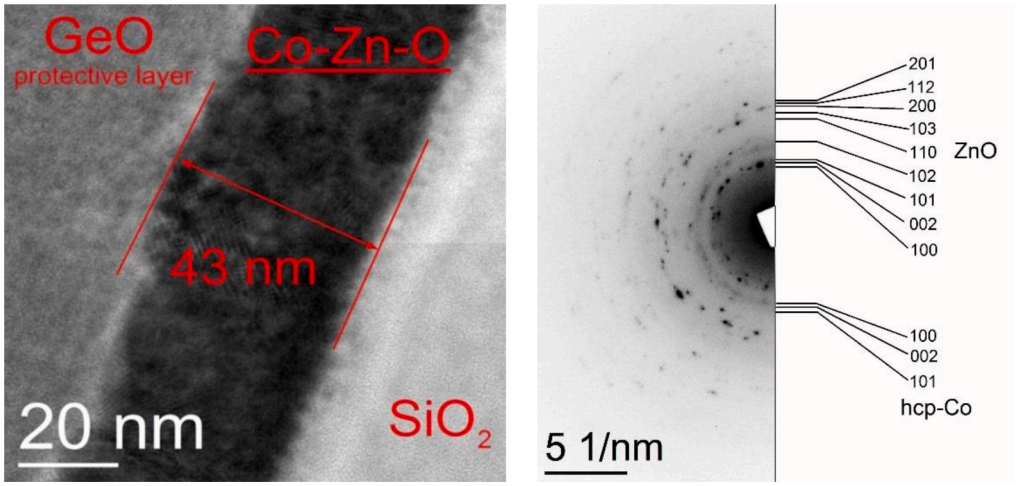

Fig. 4. Cross-section bright-field HRTEM image (left) and SAED pattern (right) for the Co-doped ZnO film at $H_2 = 30\%$ (CZO2).

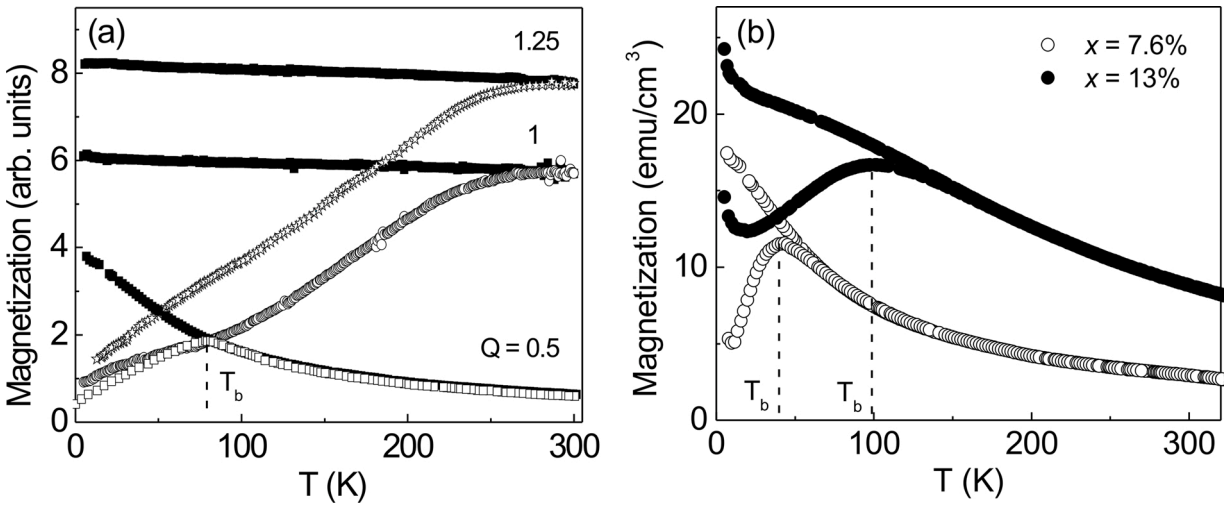

Fig. 5. FC-ZFC temperature dependences of magnetization: a – Co-NPs in SiO_2 at the ion dose of $Q*10^{17}$ ions/cm^2, H = 200 Oe; b – Co-doped ZnO films with a relative content of metallic cobalt of x, H = 100 Oe.

sample is ~ 3.9 nm at T_b = 40 K and for the CZO2 sample ~ 5.3 nm at T_b = 99 K.

Field dependences of the magnetization for the studied samples are presented in Fig. 6. It should be noted that magnetization data for the CSO samples is difficult to calculate due to the large contribution of the non-magnetic matrix. Therefore, Fig. 6a shows the field dependences of the MCD effect for the CSO samples. As mentioned above, this effect is a linear response of the magnetization and immediately excludes the contribution of a non-magnetic component. Symmetric hysteresis loops are observed with a coercive field (H_C) from 260 to 900 Oe in the case of the CSO samples. The H_C value increases with an increase in the implantation dose. The increase in H_C, as well as the samples magnetization, is associated with an increase in the number particles in the implanted layer. For the CZO samples, the field dependences of the magnetization at room temperature are presented in Fig. 6b. The CZO samples demonstrate hysteresis-free behavior of the magnetization at room temperature. This behavior is typical for both superparamagnetic particles and magnetic dilute semiconductors [9,22]. The magnetic hysteresis of the CZO samples is observed at temperatures below T_b (for example, see insert in Fig. 6b). The coercive field at T = 20 K is 130 and 245 Oe for the CZO1 and CZO2 samples, respectively.

It can be assumed that the total magnetization of the CZO samples can include magnetization from ZnO. The inclusion of a few percent of the Co^{2+} ions in the ZnO lattice can transform the paramagnetic material into a high-temperature ferromagnetic [12,13,16]. However, a ratio of the saturation magnetization at room temperature (~ 62 and ~ 104 emu/cm^3) is in good agreement with the ratio of the relative content of metallic Co in the samples (7.6% and 13%, respectively). Thus, it should be concluded that the magnetism of the samples is mainly due to Co-NPs.

The obtained magnetic data of the CSO and CZO samples indicate the absence of the oxide shell (CoO) of the included Co-NPs and/or its insignificant contribution. A thin antiferromagnetic CoO layer surrounding Co-NPs leads to the appearance of exchange anisotropy in a material [23]. This type of anisotropy causes the hysteresis loop to shift along the magnetic field axis. For the studied samples, such behavior is not observed.

The field dependences of MCD signal for the CZO samples was presented in our previous work (Fig. 8b in [16]) and are similar to the field dependence of the magnetization shown in Fig. 6b. The signal does not reach saturation up to 12 kOe that indicates a superparamagnetic nature. This behavior is justified at a blocking temperature of 40 and 99 K.

The MCD spectra for the CSO samples as well as for a 30 nm thick Co film synthesized with chemical technique are shown in Fig. 7a. It can be seen that the spectrum for the film is strikingly different from that for the nanoparticles. The MCD spectrum of the continuous Co film is characterized by a broad asymmetric positive maximum in the region of

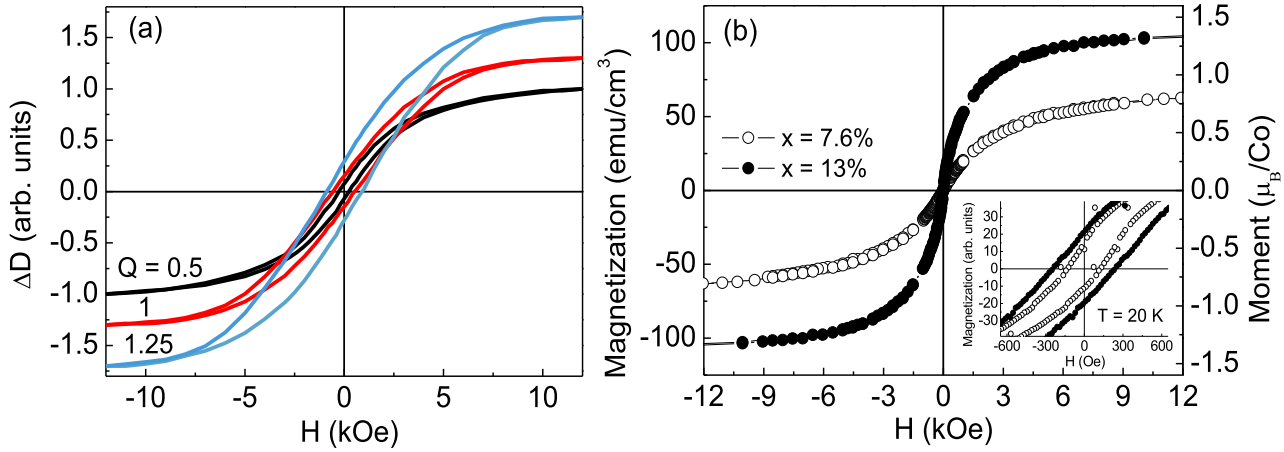

Fig. 6. a - Room temperature MCD dependences on an external magnetic field for the Co-NPs in SiO_2 at the ion dose of $Q*10^{17}$ ions/cm^2, E = 1.55 eV; b – Field dependences of the magnetization at room temperature for the Co-doped ZnO films with a relative content of metallic cobalt of x. For the Co-doped ZnO films, the contribution from the substrate was deducted. Insert: enlarged low-field parts of the field dependence of the magnetization at T = 20 K for the Co-doped ZnO films.

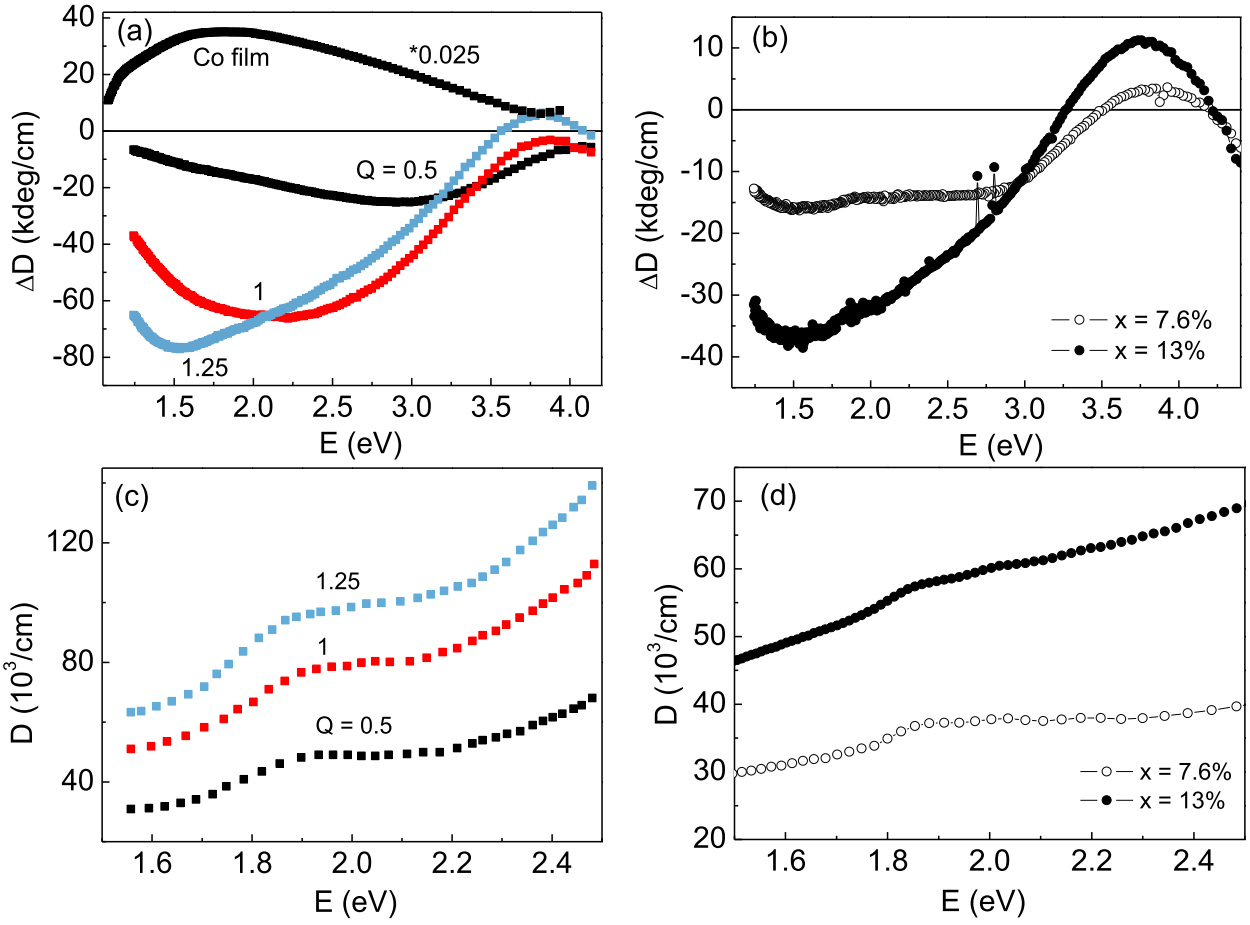

Fig. 7. Room temperature spectral dependencies of MCD (a, b) and optical density (c, d): (a, c) - Co film and the Co-NPs in SiO_2 at the ion dose of $Q*10^{17}$ ions/cm^2; (b, d) – the Co-doped ZnO films with a relative content of metallic cobalt of x. MCD effect is shown at $H = 12$ kOe. The MCD signal value for the Co film was multiplied by a factor of 0.025.

1.1–3.5 eV with a spectral gravity center of 1.8 eV (Fig. 7a). The MCD spectra for the Co-NPs are characterized also by a broad asymmetric negative maximum in the region of 1.3–3.5 eV. A spectral center of gravity for the CSO1 sample is 2.9 eV. The red-shift of the spectral center of gravity increases with an increase in the implantation dose. Besides, the MCD signal of the CSO3 sample changes sign at an energy of about 3.8 eV. A similar spectral shape has been observed for the real part of the off-diagonal component of the permittivity tensor of Co-NPs in ZrO_2 and Al_2O_3 dielectric matrices [24].

The sharp difference between the MCD spectral dependences for Co-NPs and a continuous Co film is probably due to the excitation and scattering of conduction electrons in a limited volume of cobalt nanoparticles. The Kerr effect in such materials has been studied and described in the effective medium approximation [24,25]. It was shown that the optical and magneto-optical properties of Co-NPs differ from those of the bulk Co material and depend on the nanoparticles size [24]. Despite the fact that for the sample with the highest dose, the field dependence of the magnetization is described by a curve characteristic of a thin ferromagnetic layer, the MCD spectrum of this sample is not analogous to a continuous film (Figs. 5a and 6a). Probably, the quantitative content of the particles in this sample is close to the percolation threshold. In this case, the magnetic properties of the sample are similar to a continuous ferromagnetic layer, and the MCD spectrum is determined by electronic processes in the closed volume of each particle. As a continuous medium is formed, the MCD spectrum will shift toward positive values, which corresponds to the MCD spectrum of a thin Co film (Fig. 7a).

It should be noted that the MCD spectra for the CZO samples (Fig. 7b) exhibit a shape similar to that for CSO samples. Two maxima of opposite signs are observed: a broad negative maximum in the region of 1.3–3.3 eV and a positive maximum at ~ 3.8 eV (Fig. 7b). The MCD spectra shape for these samples is in agreement with that for the CZO samples containing secondary metallic Co phase and showing clear ferromagnetic behavior at room temperature [26]. Besides, this shape is similar to the shape of the MCD spectrum measured for $[Co_{(0.6\ nm)}/ZnO_{(3\ nm)}]_{60}$ films, which include metallic Co-NPs [25].

For clarity, we presented the normalized MCD spectra for the CZO and CSO samples and compared them with each other in Fig. 8. Obviously, the spectra are in good agreement among themselves throughout the studied spectral interval. Thus, the MCD signal observed below zero for the studied CZO1 and CZO2 samples should be attributed to the Co-NPs contribution. The high-energy maximum at 3.8 eV observed in the case of CZO samples is apparently a superposition of two contributions: the Co-doped ZnO semiconductor matrix and the Co-NPs [12,13,26]. In addition, two contributions to the asymmetric negative maximum are clearly traced for all samples. The gravity center of these contributions is located at 1.5 and 2.7 eV. It is noteworthy that a redistribution of the intensity of these contributions is observed with an increase in the average particle size and the quantitative content of Co-NPs in the samples. This behavior is explained by the particle agglomeration.

The MCD spectra shape of the studied samples was also compared with that for paramagnetic [12,24] and ferromagnetic [13–15] CZO samples containing only Co^{2+} ions in the ZnO lattice. The MCD spectrum for the paramagnetic CZO sample is characterized by an s-shape feature

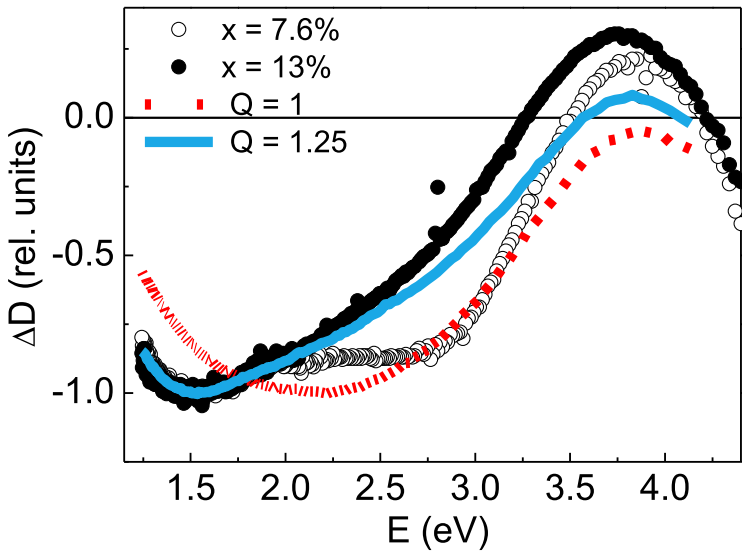

Fig. 8. Room temperature MCD spectra at $H = 12$ kOe for the Co-NPs in SiO_2 at the ion dose of $Q*10^{17}$ and the Co-doped ZnO films with a relative content of metallic cobalt of x.

near 2 eV and broad positive maximum centered at 3.4 eV [16,12,26]. At the same time, the only positive MCD signal is observed for the ferromagnetic CZO samples in the region of 1.5–3.3 eV [13–15]. The overall picture shows that the MCD spectrum shape depends on the state in which cobalt is located. Thus, the MCD spectroscopy can determine the presence of cobalt nanoparticles in various samples, in particular in Co–ZnO systems.

Finally, a large MO response from the Co-NPs in SiO_2 and ZnO matrices was traced (Fig. 7a and 7b). The MCD signal as well as total optical density of the samples were analyzed in relation to the thickness of the active layer. In the case of the CSO samples, this layer has the implanted layer thickness of 30 nm. For the CZO samples, the thickness of the active layer was equal to the films thickness (Table 1). In general, the MCD signal increases with an increase in the quantitative content of Co-NPs in the samples. The MCD value reaches ~ 77 kdeg/cm at 1.55 eV for the CSO3 sample (Fig. 4a). The MCD value at 1.55 eV for the Co-NPs in ZnO (CZO1 and CZO2 samples) is ~ 16 and ~37 kdeg/cm, respectively (Fig. 4b). An intense negative MCD signal was observed earlier for the CZO films containing metallic Co as a secondary phase [26].

A qualitative indicator is the MO activity of the material, defined as the ratio of the MCD value (ΔD) to the total optical density (D). The MO activity of the samples in the visible and near-infrared light ranges was estimated and presented in Table 2. It can be seen that some samples have a high $\Delta D/D$ value (values above 0.05 deg/kOe are in bold) at different points of the spectrum. For the Co-NPs in ZnO [26], the $\Delta D/D$ value reaches at 1.55 eV almost the limit value ($\Delta D/D = 0.1$) in a magnetic field of 10 kOe. The data obtained indicate the possibility of using the Co-NPs for the development and improvement of MO devices.

Special attention should be paid to the high-energy peak MCD observed for the CSO3 sample (Fig. 7a) as well as for all studied CZO samples (Fig. 7b). We believe that it is associated with a certain content of metallic cobalt in the samples, at which spin injection is possible. For the CZO samples, some transfer of polarized carriers from the metallic Co particles to the conducting ZnO oxide is assumed [27,28]. However, this topic is beyond the scope of this study.

Table 2
Magneto-optical activity at room temperature ($\Delta D/D$, deg/kOe) of the Co-NPs localized in matrices of various types.

Photon energy (E), eV	Co-NPs in SiO_2			Co-NPs in ZnO		Co-NPs in ZnO [26]	
	Q = 0.5	Q = 1	Q = 1.25	7.6 ± 0.9% Co	13 ±1.1% Co	1.8% Co	4.6% Co
1.55	0.027	**0.082**	**0.091**	0.040	**0.060**	**0.090**	**0.093**
2	0.027	**0.063**	**0.053**	0.029	0.041	0.013	0.040
2.5	0.026	0.043	0.029	0.027	0.026	0.035	**0.050**

4. Conclusions

The cobalt nanoparticles dispersed in a transparent dielectric SiO_2 and semiconductor ZnO matrices have been investigated. It was found that the matrix type does not affect the MCD spectrum shape of cobalt nanoparticles 4–8.5 nm in size. The MCD spectra are characterized by a broad negative maximum in the region of 1.3–3.5 eV. Two main contributions with the gravity centers at 1.5 and 2.7 eV determine the appearance of this maximum. It was revealed that the intensity of these contributions is redistributed with an increase in the average particles size and their filling density. This behavior is explained by the particles agglomeration. It was also found that the particles exhibit high (above 0.05 deg/kOe) MO activity at room temperature in the visible and near-infrared light ranges. The sharp difference between the MCD spectral dependences for the Co nanoparticles and for a continuous Co film is explained by the excitation and scattering of conduction electrons in a limited volume of cobalt nanoparticles.

In general, the obtained data, together with the literature data, made it possible to establish that the MCD spectrum shape depends on the state in which cobalt is located. This conclusion is valuable, in particular, for Co-doped ZnO films. The determination of the magnetism nature in these oxides is one of the topical problems. However, the ambiguity of opinions about the nature of this phenomenon is generated by the difficulty of determining the presence of a secondary phase in the material (X-ray diffraction, as a rule, does not reveal such phases). It is now possible to determine the presence of Co nanoparticles in Co-doped ZnO films using the MCD method.

Thus, the MCD spectroscopy in the visible and near IR ranges has proven to be a high-quality tool for detecting Co nanoparticles in materials. Moreover, Co nanoparticles dispersed in transparent matrices have shown their attractiveness as an MO controlled medium.

Declaration of Competing Interest

The authors declare no conflict of interest.

Acknowledgments

This work was supported by the Russian Science Foundation [grant number 21-72-00061]. Electron microscopic studies were carried out in the laboratory of electron microscopy of the Joint Scientific Center of the Siberian Federal University.

References

[1] A. Tamion, C. Raufast, M. Hillenkamp, E. Bonet, J. Jouanguy, B. Canut, E. Bernstein, O. Boisron, W. Wernsdorfer, V. Dupuis, Magnetic anisotropy of embedded Co nanoparticles: influence of the surrounding matrix, Phys. Rev. B 81 (2010), 144403, https://doi.org/10.1103/PhysRevB.81.144403.

[2] J. Leveneur, J. Kennedy, G.V.M. Williams, J. Metson, A. Markwitz, Large room temperature magnetoresistance in ion beam synthesized surface Fe nanoclusters on SiO_2, Appl. Phys. Lett. 98 (2011), 053111, https://doi.org/10.1063/1.3553274.

[3] M. Anand, J. Carrey, V. Banerjee, Anisotropic effect of dipolar interaction in ordered ensembles of nanoparticles, J. Mag. Mag. Mater. 454 (2018) 23, https://doi.org/10.1007/s11051-022-05424-4.

[4] M. Klimenkov, J. von Borany, W. Matz, D. Eckert, M. Wolf, K.H. Müller, Structure and magnetic properties of Co nanoclusters fabricated by ion beam synthesis in SiO_2 films, Appl. Phys. A 74 (2002) 571–575, https://doi.org/10.1007/s003390100915.

[5] D.Y. Li, Y.J. Zeng, L.M.C. Pereira, D. Batuk, J. Hadermann, Y.Z. Zhang, Z.Z. Ye, K. Temst, A. Vantomme, M.J. Van Bael, C. Van Haesendonck, Anisotropic magnetism and spin-dependent transport in Co nanoparticle embedded ZnO thin films, J. Appl. Phys. 114 (2013), 033909, https://doi.org/10.1063/1.4815877.

[6] J. Leveneur, G.V.M. Williams, D.R.G. Mitchell, J. Kennedy, Exchange bias and large room temperature magnetoresistance in ion beam-synthesized Co nanoparticles in SiO_2, Emergent Mater. 2 (2019) 313–325, https://doi.org/10.1007/s42247-019-00034-8.

[7] H. Kijima-Aoki, Ya. Endo, T. Miyazaki, T. Nojima, K. Ikeda, N. Kobayashi, Sh. Ohnuma, H. Masumoto, Shape effect of Co nanoparticles on the electric and magnetic properties of Co-SiO_2 nanogranular films, AIP Adv. 12 (2022), 035229, https://doi.org/10.1063/9.0000310.

[8] C. Clavero, B. Sepúlveda, G. Armelles, Z. Konstantinović, M. García del Muro, A. Labarta, X. Batlle, Size mediated control of the optical and magneto-optical properties of Co nanoparticles in ZrO_2, J. Appl. Phys. 100 (2006), 074320, https://doi.org/10.1063/1.2356799.

[9] I.S. Edelman, O.V. Vorotynova, V.A. Seredkin, V.N. Zabluda, R.D. Ivantsov, Yu. I. Gatiyatova, V.F. Valeev, R.I. Khaoebullin, A.L. Stepanov, Magnetic and magneto-optical properties of ion-synthesized cobalt nanoparticles in silicon oxide, Phys. Solid State 50 (2008) 2088, https://doi.org/10.1134/S1063783408110140.

[10] Sh. Ozaki, H. Kura, H. Maki, T. Sato, Size effect in magneto-optical properties of Co nanoparticle dispersed systems, J. Appl. Phys. 105 (2009), 113913, https://doi.org/10.1063/1.3125321.

[11] A.K. Zvezdin, V.A. Kotov, Modern Magneto-Optics and Magneto-Optical Materials, 1st edn., Taylor & Francis Group, New York, 1997, p. 109.

[12] Y. Fukuma, F. Odawara, H. Asada, T. Koyanagi, Effects of annealing and chemical doping on magnetic properties in Co-doped ZnO films, Phys. Rev. B 78 (2008), 104417, https://doi.org/10.1103/PhysRevB.78.104417.

[13] M. Ying, H.J. Blythe, W. Dizayee, S.M. Heald, F.M. Gerriu, A.M. Fox, G.A. Gehring, Advantageous use of metallic cobalt in the target for pulsed laser deposition of cobalt-doped ZnO films, Appl. Phys. Lett. 109 (2016), 072403, https://doi.org/10.1063/1.4961223.

[14] S. Lee, J.H. Park, B.S. Kim, D.Y. Cho, Y.N. Choi, T.W. Lee, W.K. Kim, D. Kim, Ch. R. Cho, Ch. Moriyoshi, Ch.H. Park, Y. Kuroiwa, S.Y. Jeong, Formation of ferromagnetic Co-H-Co complex and spin-polarized conduction band in Co-doped ZnO, Sci. Rep. 7 (2017) 11101, https://doi.org/10.1038/s41598-017-11078-3.

[15] G. Varvaro, A.D. Trolio, A. Polimeni, A. Gabbani, F. Pineider, C. de J. Fernaʹndez, G. Barucca, P. Mengucci, A.A. Bonapasta, A.M. Testa, Giant magneto-optical response in H^+ irradiated $Zn_{1-x}Co_xO$ thin films, J. Mater. Chem. C 7 (2019) 78, https://doi.org/10.1039/C8TC03563F.

[16] I.S. Edelman, H. Chou, Yu.E. Samoshkina, D.A. Petrov, H.C. Lin, W.L. Chan, S.-J. Sun, S.M. Zharkov, G.V. Bondarenko, M.S. Platunov, A. Rogalev, Giant hydrogen effect on the structure and physical properties of ZnO and Co-doped ZnO films fabricated by the RF magnetron sputtering in Ar + H_2 atmosphere, J. Mag. Mag. Mater. 489 (2019), 165461, https://doi.org/10.1016/j.jmmm.2019.165461.

[17] A.L. Stepanov, I.B. Khaibullin, Fabrication of metal nanoparticles in sapphire by low-energy ion implantation, Rev. Adv. Mater. Sci. 9 (2005) 109. https://www.ipme.ru/e-journals/RAMS/no_2905/stepanov.pdf.

[18] L.G. Jacobsohn, M.E. Hawley, D.W. Cooke, M.F. Hundley, J.D. Thompson, R. K. Schulze, M. Nastasi, Synthesis of cobalt nanoparticles by ion implantation and effects of postimplantation annealing, J. Appl. Phys. 96 (2004) 4444–4450, https://doi.org/10.1063/1.1787143.

[19] I.S. Edelman, D.A. Petrov, R.D. Ivantsov, S.M. Zharkov, D.A. Velikanov, G. G. Gumarov, V.I. Nuzhdin, V.F. Valeev, A.L. Stepanov, Study of morphology, magnetic properties, and visible magnetic circular dichroism of Ni nanoparticles synthesized in SiO_2 by ion implantation, Phys. Rev. B 87 (2013), 115435, https://doi.org/10.1103/PhysRevB.87.115435.

[20] B.D. Cullity, Introduction to Magnetic Materials, Addison-Wesley, Reading, MA, 1972, p. 410.

[21] N.A. Usov, M.S. Nesmeyanov, Multi-domain structures in spheroidal Co nanoparticles, Sci. Rep. 10 (2020) 10173, https://doi.org/10.1038/s41598-020-67173-5.

[22] J.M.D. Coey, J.T. Mlack, M. Venkatesan, P. Stamenov, Magnetization process in dilute magnetic oxides, IEEE Trans. Magn. 46 (2010) 2501–2503, https://doi.org/10.1109/TMAG.2010.2041910.

[23] W.H. Meiklejohn, C.P. Bean, New magnetic anisotropy, Phys. Rev. 105 (1957) 904–913, https://doi.org/10.1103/physrev.105.904.

[24] C. Clavero, G. Armelles, J. Margueritat, J. Gonzalo, M. García del Muro, A. Labarta, X. Batlle, Interface effects in the magneto-optical properties of Co nanoparticles in dielectric matrix, Appl. Phys. Lett. 90 (2007), 182506, https://doi.org/10.1063/1.2737126.

[25] E.A. Ganʹshina, M.V. Vashuk, A.N. Vinogradov, A.B. Granovsky, V.S. Gushchin, P. N. Shcherbak, Yu.E. Kalinin, A.V. Sitnikov, C.O. Kim, C.G. Kim, Evolution of the optical and magnetooptical properties of amorphous metal-insulator nanocomposites, J. Exp. Theor. Phys. 98 (2004) 1027–1036, https://doi.org/10.1134/1.1767571.

[26] Y. Fukuma, H. Asada, J. Yamamoto, F. Odawara, T. Koyanagi, Large magnetic circular dichroism of Co clusters in Co-doped ZnO, Appl. Phys. Lett. 93 (2008), 142510, https://doi.org/10.1063/1.2992631.

[27] Zh. Quan, W. Liu, X. Li, X. Xu, K. Addison, D.S. Score, G.A. Gehring, Structural and magnetotransport properties in Co/nonmagnetic films, Mater. Lett. 65 (2011) 2982–2984, https://doi.org/10.1016/j.matlet.2011.06.027.

[28] Zh. Quan, X. Zhang, W. Liu, X. Li, K. Addison, G.A. Gehring, X. Xu, Enhanced room temperature magnetoresistance and spin injection from metallic cobalt in Co/ZnO and Co/ZnAlO films, ACS Appl. Mater. Interfaces 5 (2013) 3607–3613, https://doi.org/10.1021/am303276b.